2023 IEEE International Conference on Robotics and Automation (ICRA 2023)
May 29 - June 2, 2023. London, UK

Computational Design of 3D-Printable Compliant Mechanisms with Bio-Inspired Sliding Joints

Felipe Velasquez, Bernhard Thomaszewski, and Stelian Coros
ETH Zürich

***Abstract*— We propose a computational approach for designing fully-integrated compliant mechanisms with bio-inspired joints that are stabilized and actuated by elastic elements. Similar to human knees or finger phalanges, our mechanisms leverage sliding between pairs of contacting surfaces to generate complex motions. Due to the vast design space, however, finding surface shapes that lead to ideal approximations of given target motions is a challenging and time-consuming task. To assist users in this process, our computational design tool combines forward and inverse simulation strategies that allow for guided and automated exploration of the parameter space. We demonstrate the potential of our method on a set of compliant mechanism with different joint geometries and validate our simulation results on 3D-printed prototypes.**

I. INTRODUCTION

Evolution has led to an infinite variety of designs that enable living beings to navigate through, and interact with, their environments. From wings that generate lift with minimal weight and power to human knees that last for decades and enable us to walk for hours while consuming very little energy: the solutions seen in nature are versatile, efficient, and robust. One key element for the success of these organic designs are biological joints composed of articulating surfaces with diverse geometries, enabling important functional properties such as a wide range of motion for our thumbs [1] and a variable moment arm in our knees [2]. In addition to their articulating surfaces, biological joints rely on *compliant* elements such as muscles and tendons for actuation and ligaments for stability.

While the organic designs found in nature derive their efficiency from compliance, current engineering practice in robotics is based on *rigidity*. Connections between bodies in robots are, with few exceptions, achieved with pure rotation and sliding joints. More complex movements are typically generated using linkages composed of several joints. This well-tested approach has many advantages: rigid mechanisms with conventional joints can be assembled from standardized, mass-produced, components; mathematical tools such as inverse kinematics simplify the process of generating desired motions; and computer-aided design and simulation tools facilitate their development. Nevertheless, progress in additive manufacturing now provides opportunities for case-specific joint designs that can be produced without increasing cost or complexity, leaving the design of such joints as the main challenge.

In this work, we present a computational approach to the design of compliant mechanisms with bio-inspired joints tailored for 3D printing. Similar to biological joints, we combine complex-shaped articulating surfaces in sliding contact with compliant 3D-printed springs and tensioners. Our approach builds on a versatile parametric joint description that can be adapted to meet the requirements of diverse applications.

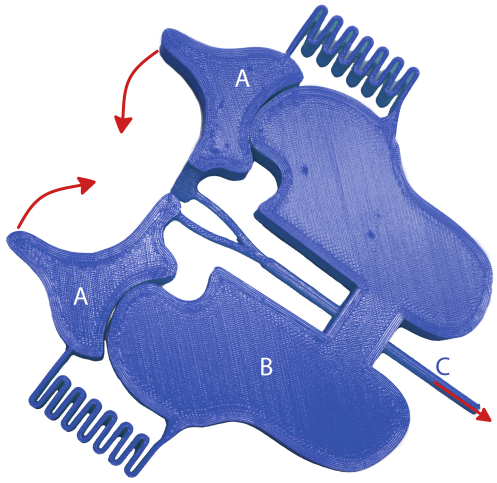

Fig. 1: A compliant gripper with bio-inspired sliding joints designed with our method. Actuating this mechanism by pulling on the center tensioner (C) generates sliding motion between the moving links (A) and the main body (B). The variable curvature of the contact surfaces effectively combines translation and rotation in a single joint.

Our forward-looking design process results in mechanisms that are fundamentally different from the traditionally-designed rigid robotic actuators. The use of additive manufacturing enables monolithic designs with integrated actuation elements that could simplify assembly. Furthermore, the ability to obtain a user-specified motion without the need for linkages composed of several moving elements illustrates one of the advantages of complex joints.

Navigating the design space of the proposed bio-inspired joints is a challenging task due to the large number of variables and their non-linear effect on the resulting behavior. We therefore propose computational tools that simplify and streamline the design process. In particular, we describe an energy minimization approach that enables accurate simulation of given joint designs. Using this forward model as a basis, we develop an optimization-driven design tool to automatically compute parameter values that lead to an ideal approximation of user-provided motions.

979-8-3503-2365-8/23/$31.00 ©2023 IEEE

As we show in our results, the combination of forward and inverse design methodologies enables user-guided and automated design exploration. We demonstrate the potential of our method by designing compliant mechanisms with different joint geometries and functionalities. We validate our designs by comparing simulation results on a set of 3D-printed prototypes.

II. RELATED WORK

There are various examples of bio-inspired joints in the literature that show how this approach can provide significant advantages when designed for specific applications. Several designs for joints mimicking the human knee have been proposed [2], [3], [4], [5]. Similar to our approach, they leverage surface contact to obtain behavior that differs from conventional joints. However, while the focus of these works is on increasing the moment arm for certain configurations, our aim is to modify the relative motion between the links.

Cuellar et al. [6] demonstrate a hand prosthesis with articulated fingers, making a compelling case for bio-inspired joints based on surface contact. However, while their joints are based on constant curvature surfaces and thus limited to pure rotation, our approach optimizes the shape of the contact surfaces such as to generate complex motion that combines rotation and translation.

3D-printed joints have received considerable attention from the research community in recent years; see, e.g., Lussenburg et al. [7] for an overview. Much of previous research [8], [9], [10] has focused on adapting existing joints for additive manufacturing. Closer to our method is the work by Liang et al. [11], who develop a general bio-inspired model based on the anatomy of the grasshopper. However, while their method is based on single point contact between convex surfaces, our approach allows for arbitrary surface pairs, thus increasing the range of motions that can be achieved.

Compliant mechanisms have been studied extensively during the past two decades [12], [13], [14], [15]. Notable examples that propose bio-inspired designs include compliant wrists [16] and monolithic arm-wings with compliant elements [17], [18]. Rather than replacing conventional revolute joints with compliant flexures, we propose an alternative approach that uses surface contact for articulation.

On a high level, our approach shares the motivation of previous work on computational mechanism design [19], [20], [21], [22], [23], i.e., to simplify and accelerate the design process of complex mechanisms. Our tool adds to this line of research by targeting the design of compliant mechanisms with contact-based joints.

III. COMPUTATIONAL MODEL

Our method builds on a bio-inspired joint model consisting of two main links, each having a complex-shaped articulating surface, as well as a compliant spring and a flexible tensioner; see Fig. 2 for an overview. Without loss of generality, we assume that one of the links is fixed while the other one moves relative to it. Actuation of the joint is achieved by pulling on the tensioner, which generates sliding motion between the links. The spring extends as the tensioner is pulled, providing an elastic force that pulls the moving link back towards its resting state while stabilizing the joint.

We define the joint geometry in two dimensions as it simplifies the analysis and simulation of the joint while preserving its kinematics. In this two-dimensional setting, we define the degrees of freedom of the moving link as $\mathbf{x} = (x, y)$ and θ. For a given material point on this link with local coordinates $\mathbf{q}_p$, we compute its position as a function of $\mathbf{x}$ and θ,

$$\mathbf{x}_{p,\text{link}} = \mathbf{x} + \mathbf{R}(\theta)\mathbf{q}_p \ , \tag{1}$$

where $\mathbf{q}_p = \mathbf{x}_{p,0} - \mathbf{x}_0$ and $\mathbf{R}(\theta)$ is the 2D rotation matrix,

$$\mathbf{R}(\theta) = \begin{bmatrix} \cos(\theta) & -\sin(\theta) \\ \sin(\theta) & \cos(\theta) \end{bmatrix} \ . \tag{2}$$

This relationship is used to track the position of all relevant points on the moving link ($\mathbf{x}_{*,\text{link}}$) that will be introduced in the following sections.

A. Kinematics Simulation

We simulate the kinematic behavior of our mechanisms by solving a series of static equilibrium problems corresponding to different tensioner lengths. For each step $i \in 1, 2, ..., N_{pos}$, the configuration of the mechanism $(\mathbf{x}_i^*, \theta_i^*)$ is found by minimizing the potential energy of the spring subject to a set of constraints,

$$\begin{aligned} \mathbf{x}_i^*, \theta_i^* = \underset{\mathbf{x},\theta}{\text{argmin}}\, E(\mathbf{x}, \theta) \quad s.t \\ g(\mathbf{x}, \theta) = 0 \\ \mathbf{h}(\mathbf{x}, \theta) \geq 0 \ , \end{aligned} \tag{3}$$

where

$$E(\mathbf{x}, \theta) = \frac{1}{2} k \Delta l_s(\mathbf{x}, \theta)^2 \ , \tag{4}$$

and

$$\Delta l_s(\mathbf{x}, \theta) = \|\mathbf{x}_{s,\text{link}}(\mathbf{x}, \theta) - \mathbf{x}_{s,\text{fixed}}\| - l_{0,s} \ . \tag{5}$$

The constraint $g(\mathbf{x}, \theta) = 0$ enforces the length of the tensioner $l_{t,i}$ for step i by computing the distance between the fixed point $\mathbf{x}_{t,\text{fixed}}$ and the moving end $\mathbf{x}_{t,\text{link}}(\mathbf{x}, \theta)$ as

$$g(\mathbf{x}, \theta) = \|\mathbf{x}_{t,\text{link}}(\mathbf{x}, \theta) - \mathbf{x}_{t,\text{fixed}}\| - l_{t,i} \ . \tag{6}$$

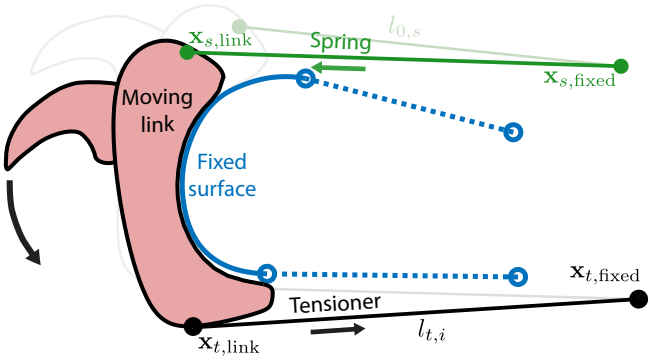

Fig. 2: Schematic view of our bio-inspired joint model. Arrows indicate direction of movement when actuated.

Reducing the value of $l_{t,i}$ in each step i emulates the effect of pulling on the tensioner, which simulates the process of actuation. The inequality constraints $\mathbf{h}(\mathbf{x}, \theta) \geq 0$ model the contact between the links as explained next.

B. Contact Constraints

During operation of the mechanism, the points of contact between the two surfaces are constantly changing. This means that the constraints in (3) must allow for the two surfaces to make contact and separate at any location. We model these conditions by discretizing the surface of the moving link into N_m points $\mathbf{x}_{\text{link},j}$, and enforcing the minimum signed distance from these points to the fixed surface to be non-negative,

$$h_j(\mathbf{x}, \theta) = \left(\mathbf{x}_{\text{link},j} - \mathbf{x}^*_{f,j}\right) \cdot \hat{\mathbf{n}}_{f,j} \geq 0 \ , \tag{7}$$

where $\mathbf{x}^*_{f,j}$ is the nearest point to $\mathbf{x}_{\text{link},j}$ on the fixed surface and $\hat{\mathbf{n}}_{f,j}$ is the unit surface normal at point $\mathbf{x}^*_{f,j}$. See Fig. 3 for an illustration.

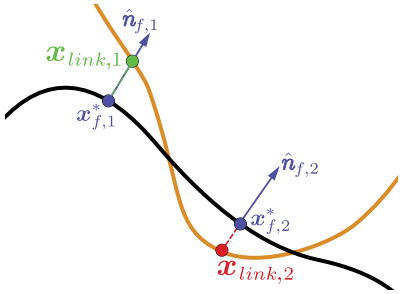

Fig. 3: Visualization of the signed minimum distance between two points on the moving link (*orange*) and the fixed surface (*black*). The green point fulfills the contact constraint ($h(\mathbf{x}_{\text{link},1}) > 0$) while the red point does not ($h(\mathbf{x}_{\text{link},2}) < 0$).

IV. OPTIMIZATION-DRIVEN DESIGN

Our simulation model allows users to predict the joint kinematics of any given design without the need to manufacture it. However, the working principle of our contact-based joints makes it non-trivial to find designs that exhibit specific behaviors. It is therefore of great value to combine simulation capabilities with design exploration and automation tools that help users in creating joints that fulfill their requirements.

A. Design Variables

All parameters included in the simulation model could, in principle, be used as design variables in the optimization tool. These include the geometry of the contact surfaces, the fixation points for the spring and the tensioner, the relative location of the trajectory tracking point with respect to the sliding surface, and the range of reduction of the tensioner length. To demonstrate the capabilities of our approach, we chose to focus on the geometry of the contact surfaces. The corresponding design variables have a significant but not necessarily intuitive impact on the resulting trajectories.

Both of the contact surfaces are modeled as splines constructed through 2D polynomial interpolation of a set of control points. This allows us to obtain smooth, complex-shaped surfaces with a relatively small number of control variables. We collect these control points in a vector $\mathbf{p}$ that is passed to the design optimization algorithm, which is described next.

B. Objective Function

Automated design exploration is performed by formulating an optimization problem, which seeks to find design variables $\mathbf{p}^*$ that lead to an ideal approximation of the desired joint movement. This requires defining an objective function $f(\mathbf{p})$ that measures the difference between the trajectory of a given tracked point and its target motion. To this end, we define the target trajectory through a set of points $\mathbf{X}_{\text{target}} \in \mathbb{R}^{2\times N_{\text{target}}}$. We then construct a spline $\mathbf{s}(t)$ that smoothly interpolates the simulated trajectory points $\mathbf{X}(\mathbf{p}) \in \mathbb{R}^{2\times N_{pos}}$. This smooth representation allows us to compute the nearest point on the spline $\mathbf{s}(t^*_k)$ to each point $\mathbf{x}_{\text{target},k}$. Finally, we define the difference between the target and the current trajectory as

$$f(\mathbf{p}) = \sum_{k=1}^{N_{\text{target}}} \left\|\mathbf{s}(t^*_k) - \mathbf{x}_{\text{target},k}\right\|^2 \ . \tag{8}$$

Defining the objective function in this way ensures that the optimal solution $\mathbf{X}(\mathbf{p}^*)$ is as close as possible to all points in $\mathbf{X}_{\text{target}}$ without enforcing the simulated trajectory to start or end at the same points as the target.

C. Robustness

Our design optimization algorithm utilizes the simulation model from section III in its inner loop to evaluate candidate solutions. This evaluation is itself a non-trivial minimization problem and we observed that the optimizer can sometimes reach parameter values $\mathbf{p}'$ for which the simulation model fails to converge. To avoid such failures, we include two additional terms in our objective function (10), penalizing solutions that do not satisfy the optimality conditions for Eq. (3). The first penalty term V_i sums the maximum constraint violations, while the second term R_i sums the residuals of the first order optimality conditions for each equilibrium configuration $\mathbf{x_i}(\mathbf{p})$.

During testing we also observed results with unstable sections in which the moving link would jump between stable states. Such solutions are undesirable as the joint cannot be held in a position within the unstable range. We therefore included an additional term ΔW_i in the objective function to penalize such solutions. An unstable section is characterized by requiring significantly less work to move between configurations relative to the work required in stable sections. Therefore, ΔW_i should penalize the difference in work required to move from x_{i-1} to x_i and the work required to move from x_{i-2} to x_{i-1}, i.e.,

$$\Delta W_i = \left(\Delta E_i - \Delta E_{i-1}\right)^2 = \left(E_i - 2E_{i-1} + E_{i-2}\right)^2 \ . \tag{9}$$

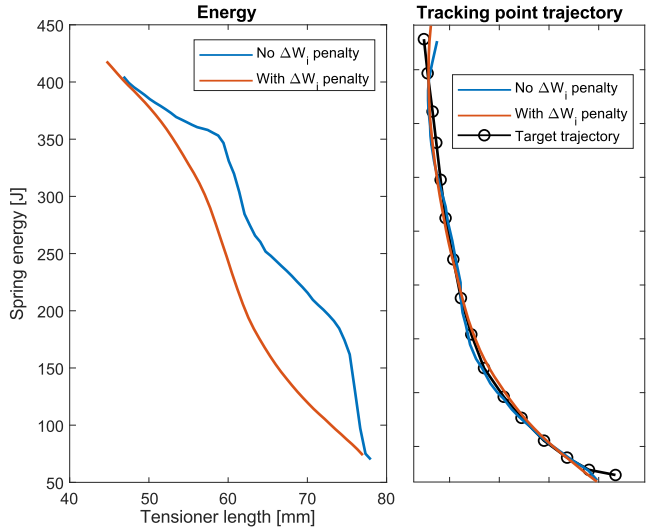

Fig. 4: Effect of the penalty term ΔW_i on the optimal trajectory and its corresponding energy profile. The penalty term leads to significantly improved smoothness in the energy profile while having little impact on trajectory approximation.

We combine all penalty terms with the trajectory matching term into a compound objective function

$$f(\mathbf{p}) = \frac{1}{L_T N_{\text{target}}} \sum_{k=1}^{N_{\text{target}}} \|\mathbf{s}(t_k^*) - \mathbf{x}_{\text{target},k}\|^2 + \frac{1}{N_{pos}} \left(\sum_{i=1}^{N_{pos}} w_V \frac{V_i}{L_T} + w_R \frac{R_i}{L_T} + \sum_{i=3}^{N_{pos}} w_W \Delta W_i \right), \tag{10}$$

where w_V, w_R, and w_W are coefficients defining the relative importance of the penalty terms and L_T denotes the total length of the target trajectory. We found that setting $w_V = 1 \times 10^1$, $w_R = 1 \times 10^{-3}$ and $w_W = 2 \times 10^{-7}$ led to good trajectory matching while preventing jumps and convergence problems (see Fig. 4). Currently, the procedure to set these weights is based on manual iteration in response to undesirable behavior. However, the values listed above worked well for all of the examples that were tested indicating a low sensitivity of the solution to variations of these weights. Finally, to solve the resulting optimization problem, we use the Nelder-Mead Simplex algorithm available in Matlab's *fminsearch* [24].

D. Interactive Exploration

Our optimization-driven design tool enables automated discovery of novel joint geometries from high-level user input. As a complement to this automatic approach, we also developed an interactive design tool that allows for guided, simulation-based design exploration. Using this tool, designers can interactively modify joint geometries and rapidly visualize the corresponding changes in mechanism kinematics. To this end, we use a pre-computed numerical estimate of the Jacobian of the mechanism's trajectory to predict changes that would be generated while the user modifies control points of the contact surfaces. Each time the user decides to test a promising design modification, a complete simulation is executed and the process continues until a satisfying solution is found. The user can also interactively specify target trajectories at any time and run the optimization-driven algorithm.

V. Results

We demonstrate the potential of our computational design tool on two compliant mechanisms, each exhibiting bio-inspired joints with complex contact surfaces. In the first example, we show how our optimization-driven design tool enables automated discovery of joint geometries that closely reproduce a given target trajectory. In the second example, we present a versatile gripper mechanism with a variable center of rotation designed using our simulation tools. We furthermore validate our simulation model by comparing predicted trajectories to experimentally acquired data.

A. Manufacturing

For manufacturing, the 2D geometry is extruded in the direction normal to the plane to obtain a 3D model. The resulting 3D geometry is manufactured in a single operation with fused filament fabrication (FFF) or stereolithography (SLA) based printers. This is accomplished by fabricating the entire mechanism from a material with high elongation at break and low friction such as Markforged's Nylon [25], Formlab's Durable resin [26], or TPU A95 [27]. With this approach, the desired elongation range and stiffness for the spring are obtained by modifying its geometry parameters such as the frequency of undulation and the length of each segment.

All of our examples are 3D printed in a single process and require no assembly or manual processing other than removal of support material. The 3D models were created from the DXF output of the simulation tool using standard CAD software. The white colored designs were printed using Markforged Nylon and the blue colored prints were created using 3DJAKE TPU A95.

B. Trajectory Matching for a Claw

A considerable challenge in designing compliant mechanisms with bio-inspired, contact-based joints is to find design variables that best approximate given target motions. In this example, we use our optimization-driven design tool to modify the contact surfaces of the Claw model shown in Fig. 2. To this end, we define a target trajectory for the tip of the claw that combines linear motion and rotation with a variable center of rotation—a motion that cannot be accomplished with a single conventional joint. Fig. 5 shows the target trajectory (black), the original trajectory of the claw (blue), and the trajectory generated by the result of the optimization tool (orange).

Fig. 6 shows an overlay of the trajectory of the claw mechanism and the optimized, 3D printed prototype. Even though both contact surfaces were convex in the initial design (Fig. 2), our optimization tool discovered a non-convex

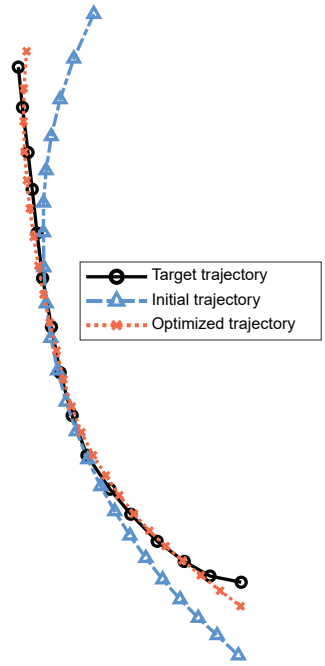

Fig. 5: Claw-tip trajectories.

surface that leads to a surprisingly accurate approximation of the target motion. This highly non-linear relation between joint geometry and kinematics highlights the challenge of manual design.

C. Gripper

The gripper mechanism shown in Fig. 7 provides another example for how our methodology can generate novel and functional designs. In this case, the simulation-based design exploration approach was used to quickly test the behavior of several geometries when gripping objects of different size. Once a design with satisfying performance was found in simulation, we printed a physical prototype for validation. As predicted, the varying contact points between the surfaces allow the mechanism to grip objects in the range of $40mm$ to $< 1mm$.

D. Experimental Validation

To validate our simulation model, we compared its results to motion capture data from a 3D printed prototype of our Claw-like mechanism (Fig. 8). The experiment consisted of recording 6 sequential actuations of the prototype, pulling on the tensioner manually and slowly releasing the tension such that the spring restores the moving link to its starting position. Video frames were then analyzed using the *Tracker* software to extract time varying x-y coordinates of the tracking points. Finally, to compare with the simulation, the trajectory of the tip was computed in Matlab. Segments where the pulling force on the tensioner was too low to keep the surfaces in contact were excluded as the simulation is designed to start with enough tension to make the surfaces touch. It can be seen from the trajectories shown in Fig. 8 that the simulation accurately matches the motion of

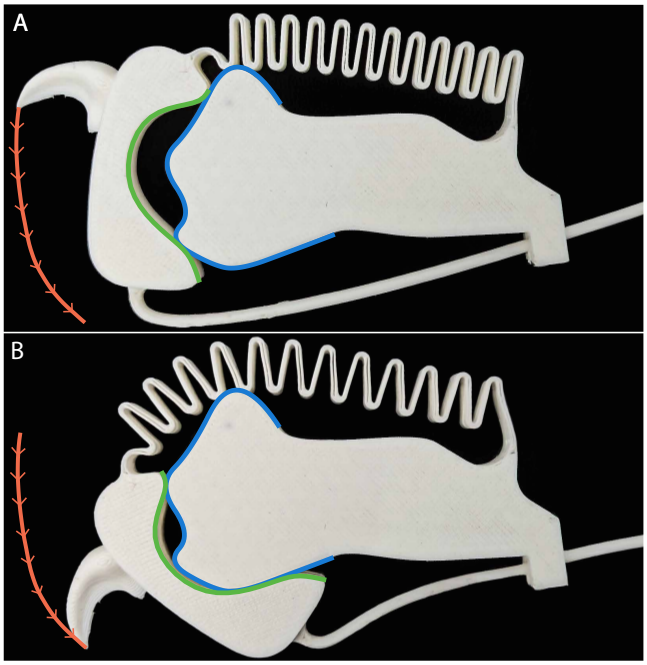

Fig. 6: 3D printed prototype of the optimized Claw mechanism in its initial (A) and fully actuated (B) configuration. The geometry obtained from the optimization process is indicated in green (moving link) and blue (fixed link) color, respectively. The simulated trajectory is shown in orange.

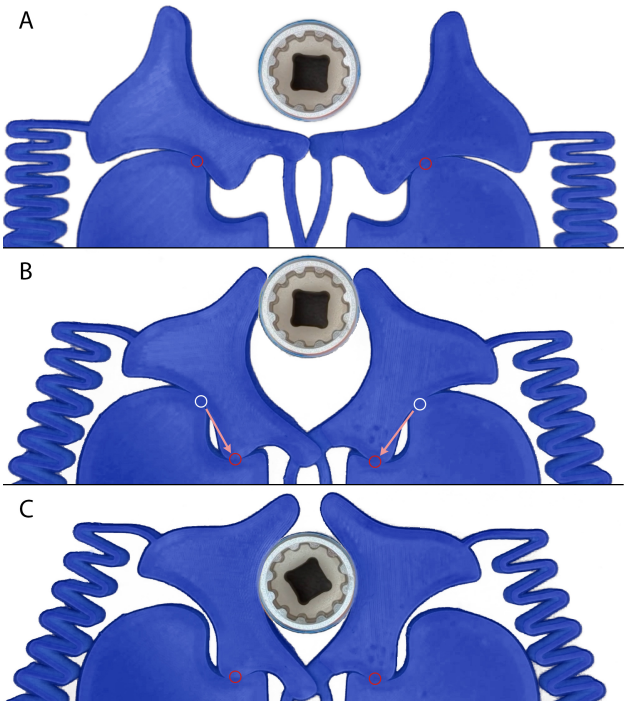

Fig. 7: 3D printed prototype of the gripper in 3 positions during operation (grabbing a 12mm socket). The non-convex surface of the body allows the center of rotation of the moving links to change substantially between the large (A) and small (C) object gripping configurations.

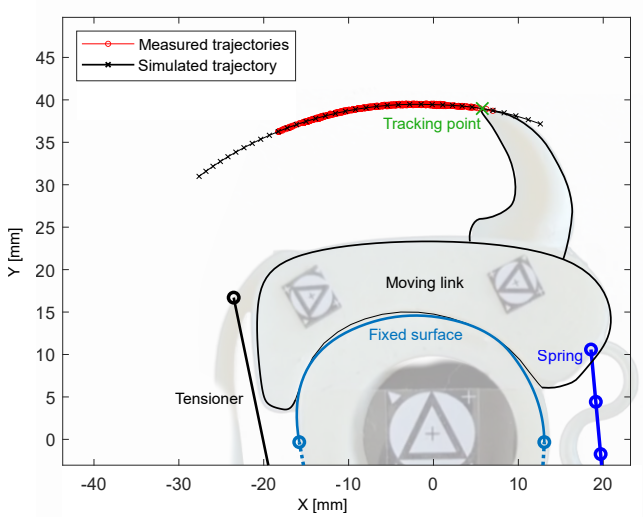

Fig. 8: X-Y comparison plot of simulated and measured trajectories with the simulation model superimposed on the 3D printed prototype.

the physical joint. The mean distance between measured positions and the simulated trajectory is $0.048mm$ with a standard deviation of $0.030mm$, comparing these values to the length of the trajectory ($42.3mm$) validates the capability of the simulation model to estimate the behavior of a given joint design.

VI. DISCUSSION

The two examples presented in the previous section show the ability of our approach to create mechanisms that utilize complex surfaces to combine rotation and translation in a single joint. The Claw example shows how this capability can be leveraged to generate a trajectory with a significant increase in curvature along its path. Furthermore, the Gripper takes advantage of non-convex contact surfaces by providing a second pivot point near the end of the closing operation (Fig. 7-C). This allows the moving links to rotate towards each other to firmly grab objects. Nevertheless, taking full advantage of the functionality of our bio-inspired joints is a challenging task. Unlike conventional joints, the geometry of these contact surfaces does not have an intuitive relation to the resulting motion of the mechanism. The interactive and automated design tools we presented in this work are therefore crucial ingredients for creating successful designs.

A. Limitations

A main limitation of our approach is the difficulty of predicting in advance to what extent a desired trajectory can be approximated. Fig. 5 shows how, even though the geometry of the Claw was optimized to match the target trajectory, it fails to do so near the bottom right. In this case, the change in curvature was greater than what could be obtained from the sliding surface pair while remaining smooth and keeping the trajectory free of jumps.

Our simulation model also presents opportunities for improvements. First, the spring and tensioner models do not take into account the energy required to bend the 3D printed elements. Even though the magnitude of this energy is relatively small compared to the energy required to elongate the spring, it can lead to discrepancies between the simulated and 3D printed models. Second, the execution time for the forward model is on the order of seconds. This not only hampers the experience of interactive design but also translates into multi-hour execution times for our optimization-driven design tool.

B. Future work

A natural extension to our approach would be to allow for the design of 3D surfaces and non-planar trajectories, enabling motion similar to, e.g., human thumbs. Furthermore, adding force and torque computations would provide meaningful information for the design of functional mechanisms, this could then be extended to compute the requirements for motorized actuation. Finally, other objective functions could be implemented to automate the design of mechanisms with different purposes such as variable moment-arm joints, multistable mechanisms or even joints with intentional hysteresis between directions of motion.

REFERENCES

[1] E. Halilaj, M. J. Rainbow, C. Got, J. B. Schwartz, D. C. Moore, A. P. C. Weiss, A. L. Ladd, and J. J. Crisco, "In vivo kinematics of the thumb carpometacarpal joint during three isometric functional tasks," in *Clinical Orthopaedics and Related Research*, vol. 472, no. 4. Springer New York LLC, 2014, pp. 1114–1122.

[2] A. C. Etoundi, R. Vaidyanathan, and S. C. Burgess, "A bio-inspired condylar hinge joint for mobile robots," *IEEE International Conference on Intelligent Robots and Systems*, pp. 4042–4047, 2011.

[3] S. C. Burgess and A. C. Etoundi, "Performance maps for a bio-inspired robotic condylar hinge joint," *Journal of Mechanical Design, Transactions of the ASME*, vol. 136, no. 11, pp. 1–7, 2014.

[4] A. G. Steele, A. Hunt, and A. C. Etoundi, "Development of a bio-inspired knee joint mechanism for a bipedal robot," in *Conference on Biomimetic and Biohybrid Systems*, 2017, pp. 418–427.

[5] F. Russell, Y. Zhu, W. Hey, R. Vaidyanathan, and P. Ellison, "A biomimicking design for mechanical knee joints," *Bioinspiration and Biomimetics*, vol. 13, no. 5, 2018.

[6] J. S. Cuellar, D. Plettenburg, A. A. Zadpoor, P. Breedveld, and G. Smit, "Design of a 3D-printed hand prosthesis featuring articulated bio-inspired fingers," *Proceedings of the Institution of Mechanical Engineers, Part H: Journal of Engineering in Medicine*, vol. 235, no. 3, pp. 336–345, 2021.

[7] K. Lussenburg, A. Sakes, and P. Breedveld, "Design of non-assembly mechanisms: A state-of-the-art review," *Additive Manufacturing*, vol. 39, no. January, 2021.

[8] J. S. Cuellar, G. Smit, D. Plettenburg, and A. Zadpoor, "Additive manufacturing of non-assembly mechanisms," *Additive Manufacturing*, vol. 21, pp. 150–158, 2018.

[9] J. Calì, D. A. Calian, C. Amati, R. Kleinberger, A. Steed, J. Kautz, and T. Weyrich, "3D-printing of non-assembly, articulated models," *ACM Transactions on Graphics*, vol. 31, no. 6, pp. 1–8, 2012.

[10] X. Song and Y. Chen, "Joint design for 3-d printing non-assembly mechanisms," *Proceedings of the ASME Design Engineering Technical Conference*, vol. 5, no. August 2012, pp. 619–631, 2012.

[11] R. Liang, G. Xu, Z. Teng, M. Li, S. Zhang, X. Zheng, K. Zhang, and B. He, "A General Arthropod Joint Model and its Applications in Modeling Human Robotic Joints," *IEEE Access*, vol. 9, no. February, pp. 7814–7822, 2021.

[12] L. L. Howell, S. P. Magleby, and B. M. Olsen, *Handbook of Compliant Mecahnisms*, 2019, no. 2013.

[13] A. Zolfagharian, M. Lakhi, S. Ranjbar, Y. Tadesse, and M. Bodaghi, "3D printing non-assembly compliant joints for soft robotics," *Results in Engineering*, vol. 15, p. 100558, 2022. [Online]. Available: https://www.sciencedirect.com/science/article/pii/S2590123022002286

[14] R. R. Ma, L. U. Odhner, and A. M. Dollar, "A modular, open-source 3D printed underactuated hand," *Proceedings - IEEE International Conference on Robotics and Automation*, pp. 2737–2743, 2013.

[15] A. Bruyas, F. Geiskopf, and P. Renaud, "Towards statically balanced compliant joints using multimaterial 3D printing," *Proceedings of the ASME Design Engineering Technical Conference*, vol. 5A, pp. 1–10, 2014.

[16] P. Bilancia, M. Baggetta, G. Berselli, L. Bruzzone, and P. Fanghella, "Design of a bio-inspired contact-aided compliant wrist," *Robotics and Computer-Integrated Manufacturing*, vol. 67, 2020.

[17] E. Sihite, P. Kelly, and A. Ramezani, "Computational Structure Design of a Bio-Inspired Armwing Mechanism," *IEEE Robotics and Automation Letters*, vol. 5, no. 4, pp. 5929–5936, 2020.

[18] V. Megaro, J. Zehnder, M. Bächer, S. Coros, M. Gross, and B. Thomaszewski, "A computational design tool for compliant mechanisms," *ACM Transactions on Graphics*, vol. 36, no. 4, 2017.

[19] S. Coros, B. Thomaszewski, G. Noris, S. Sueda, M. Forberg, R. W. Sumner, W. Matusik, and B. Bickel, "Computational design of mechanical characters," *ACM Transactions on Graphics (TOG)*, vol. 32, no. 4, pp. 1–12, 2013.

[20] B. Thomaszewski, S. Coros, D. Gauge, V. Megaro, E. Grinspun, and M. Gross, "Computational design of linkage-based characters," *ACM Transactions on Graphics (TOG)*, vol. 33, no. 4, pp. 1–9, 2014.

[21] M. Bächer, S. Coros, and B. Thomaszewski, "LinkEdit: Interactive linkage editing using symbolic kinematics," *ACM Transactions on Graphics*, vol. 34, no. 4, pp. 1–8, 2015.

[22] T. Takahashi, J. Zehnder, H. G. Okuno, S. Sugano, S. Coros, and B. Thomaszewski, "Computational Design of Statically Balanced Planar Spring Mechanisms," *IEEE Robotics and Automation Letters*, vol. 4, no. 4, pp. 4438–4444, 2019.

[23] L. Zhu, W. Xu, J. Snyder, Y. Liu, G. Wang, and B. Guo, "Motion-guided mechanical toy modeling," *ACM Transactions on Graphics*, vol. 31, no. 6, 2012.

[24] MATHWORKS, "Optimizing Nonlinear Functions - MATLAB & Simulink," 2022. [Online]. Available: https://ch.mathworks.com/help/releases/R2022a/matlab/math/optimizing-nonlinear-functions.html

[25] Markforged, "Material Datasheet Composites," 2021.

[26] I. Fomlabs, "Durable Resin for Pliable Prototyping Datasheet," 2020.

[27] 3DJAKE, "TPU A95 Orange," 2022. [Online]. Available: https://www.3djake.com/3djake/tpu-a95-orange